

Synchronization of elastically coupled processive molecular motors and regulation of cargo transport

Felix Kohler* and Alexander Rohrbach†

Laboratory for Bio- and Nano-Photonics, Department of Microsystems Engineering—IMTEK, University of Freiburg, Germany
and Centre for Biological Signalling Studies (bioss), University of Freiburg, Germany

(Received 9 July 2013; published 6 January 2015)

The collective work of motor proteins plays an important role in cellular transport processes. Since measuring intermotor coupling and hence a comparison to theoretical predictions is difficult, we introduce the synchronization as an alternative observable for motor cooperativity. This synchronization can be determined from the ratio of the mean times of motor resting and stepping. Results from a multistate Markov chain model and Brownian dynamics simulations, describing the elastically coupled motors, coincide well. Our model can explain the experimentally observed effect of strongly increased transport velocities and powers by the synchronization and coupling of myosin V and kinesin I.

DOI: [10.1103/PhysRevE.91.012701](https://doi.org/10.1103/PhysRevE.91.012701)

PACS number(s): 87.16.Nn, 87.10.Mn, 87.15.hj, 87.16.ad

I. INTRODUCTION

In biological systems, energetic processes are typically “quantized” by the hydrolysis of adenosine triphosphate (ATP) molecules enabling elementary reactions and conformation changes of proteins [1,2]. In this way, molecular motors step discontinuously along cytoskeletal filaments in order to transport cargos such as vesicles or to translate filaments for cytoskeletal reorganization [1]. Most motors operate in groups and thereby enable a more efficient cargo transport [3–7]. However, the observable fingerprints of the quantization, the stepwise movement of the cargo, remains hidden. Only a few studies have shown coordinated and coherent stepping of motors *in vitro* [8,9] and *in vivo* [10,11], revealing a synchronization between the proteins by tracking either the motors or the cargo. However, in general it is very difficult to measure the degree of coupling between the motors, which complicates the comparison of experimental and theoretical results. Therefore, alternative observables for motor coupling need to be developed theoretically that are also accessible by experiments. For the transport velocity of cooperative motors both an increase [12] and decrease [13] in comparison to measured individual motor velocities could be observed in *in vitro* motility assays. However, theoretical models covering both effects are still missing. Cargo transport by elastically coupled motors has been investigated theoretically with special emphasis on unbinding or binding effects, assuming a simplified velocity-force relationship and state-transition models for specific motors [14–20]. In other studies, the downhill diffusion in periodic energy landscapes for more generalized systems and couplings were calculated to estimate quantities like transport velocities or efficiencies [21–25]. The problem with these studies is that the observables for cooperative processes typically result from ensemble averages, and the mutual interferences between the motors are difficult to determine.

Here, we provide an innovative description of motor stepping and resting, which allows us to determine the intermotor coupling. In particular, we investigate the degree of synchronization q for elastically coupled motors stepping

in a coordinated manner during cargo transport. q helps to identify coupled processes, which are often covered in a diffusion governed environment and which are difficult to extract from measured fluctuation time series. We show that q is determined by the parameters characterizing the protein’s specific free potential energy landscape such as step size or stall force, which differ strongly for different motor proteins. We assume the motors to be infinitely processive corresponding to the long run lengths of proteins like myosin V or kinesin I [26–28]. Using a Markov chain model, the synchronization is defined by the probability to find the coupled N -motor system in its ground state. By considering the occupation of higher energy states, we derive the nonlinear behaviors of transport powers and velocities as a function of external loading, as well as a resonantlike behavior of the transport velocity as a function of coupling strength, which enables insights into transport regulation processes. For comparison, we performed Brownian dynamics simulations illustrating the discontinuous cargo transport and the possibility of an alternative measure for coupled molecular motors.

II. RATE MODEL FOR MOTOR COUPLING

A. Description of single motor stepping

A step of a processive molecular motor, i.e., one mechanochemical cycle, includes the unbinding of one head of the motor, the hydrolysis of ATP, the power stroke of the other motor head, the diffusive search of the next binding site by the new leading head, and the rebinding to the filament [Fig. 1(a)]. In the model presented here, such a step is described by the diffusion from one local minimum in a motor-specific potential landscape over a barrier to another minimum [Fig. 1(b)] [1,2]. The tilt of the potential originates from ATP hydrolysis. Assuming the frequent case of tight chemical coupling, where one ATP is consumed per cycle, the free energy difference between two consecutive minima $\Delta V_{\text{ATP}} = \Delta G_{\text{ATP}} \eta_{\text{TD}}$ is given by the Gibbs free energy ΔG_{ATP} released per ATP molecule under typical cellular conditions [29] times a maximal thermodynamic efficiency η_{TD} to transform this energy into mechanical work. The distance between two potential minima is given by the intrinsic step size s_m of the molecular motor. The sensitivity of the

*felixkohler@gmail.com

†rohrbach@imtek.de

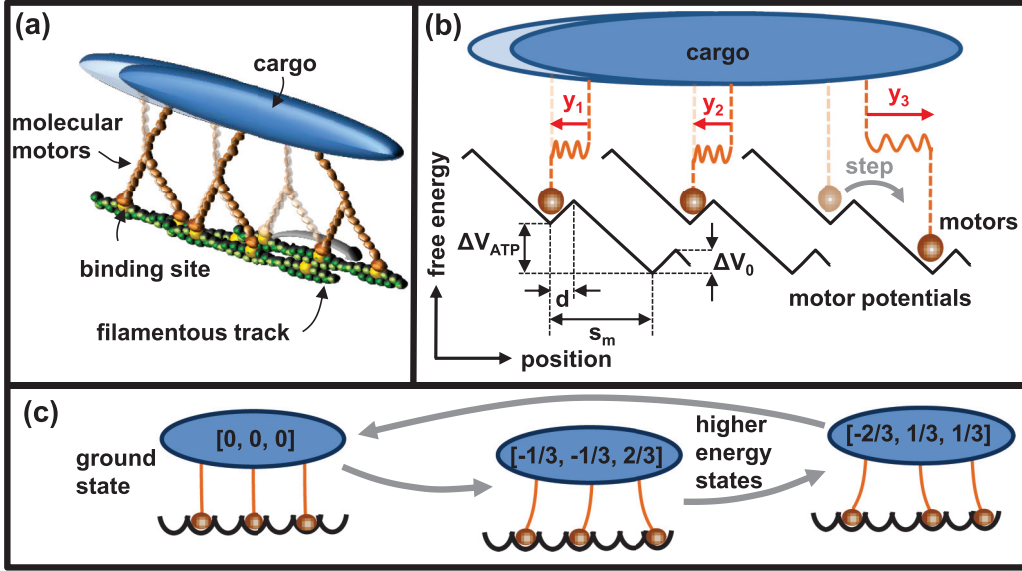


FIG. 1. (Color online) (a) Sketch of motor cluster pulling on a cargo before (transparent) and after (opaque) one motor performs a step. (b) Mechanistic model for motor based cargo transport visualizing the parameters ΔV_0 , d , s_m , and ΔV_{ATP} and the relative motor positions $y_i = y_{\text{int},i} + y_{\text{ext},i}$. (c) Illustration of the ground state (lowest internal strain) and two higher-energy states following a Markov chain. The states are characterized by the set of normalized deflections $y_{\text{int},i}/s_m = [y_{\text{int},1}/s_m, y_{\text{int},2}/s_m, y_{\text{int},3}/s_m]$ generated by internal forces.

motor to external forces is controlled by the distance parameter d between the potential minimum and the potential barrier of height ΔV_0 . The parameters s_m , ΔV_0 , ΔV_{ATP} , and d are illustrated in Fig. 1(b) and are specific for the respective motor protein. The detailed shape of this potential is usually unknown and differs for the various types of processive motor proteins.

B. Multiple motors

In our model, a step of a molecular motor is described by a diffusion over a potential barrier. According to Kramers' theory, the rate of such a stochastic process is $r = r_0 e^{(-\Delta V/k_B T)}$, where the prefactor r_0 depends on the diffusivity and the actual shape of the potential [30,31]. A force applied to a motor will affect the probability of this motor to perform a step [1,32,33]. Here, each motor is coupled to a common cargo by the linear force $F_{c,i}(y_i) = \kappa_m y_i(t)$, where y_i denotes the motor deflection from its relaxed position, i.e., $y_i = 0$ [Fig. 1(b)]. The stiffness κ_m of the linkage includes multiple sources of compliance, such as stretching of the motors, stretching of scaffold proteins linking the motors to the cargo, and deformation of the cargo itself. Therefore, it can vary significantly in different cellular systems and in *in vitro* approaches [7,34,35]. A motor's deflection $y_i = y_{\text{int},i} + y_{\text{ext},i}$ can result from two forces $F_{c,i} = F_{\text{int},i} + F_{\text{ext}}/N$ exerted by the cargo on a motor: an internal force $F_{\text{int},i}(t) = \kappa_m y_{\text{int},i}(t)$ generated by the other motors connected to the same cargo and an external force $F_{\text{ext}}(t)$ acting on the cargo, which is distributed over all motors involved. Here, $y_{\text{int},i}(t)$ denotes the motor deflection by internal forces, without external load. The deflection $y_{\text{ext},i}(t) = \frac{1}{N} F_{\text{ext}}/\kappa_m$ results from the external force. The force $F_{c,i}$ leads to a change of the overall potential each motor is diffusing in. The main effect of this potential change is the variation of the height of each motor's potential barrier $\Delta V_0 \rightarrow \Delta V_i = \Delta V_0 + (\Delta V_{\text{ext}} + \Delta V_{\text{int},i})$, which results from an external force acting on the cargo $\Delta V_{\text{ext}} = -\frac{1}{N} d F_{\text{ext}}$ and

from the influence of other motors pulling on the cargo $\Delta V_{\text{int},i} = \frac{\kappa}{2} d^2 + \kappa y_{\text{int},i} d$ (SM1 in the Supplemental Material [36]). The effective interaction stiffness is $\kappa(N) = \frac{N-1}{N} \kappa_m$ in the low friction limit and $\kappa = \kappa_m$ for high cargo friction (SM1 in Ref. [36]). The friction and thereby κ scale with the cargo size. Considering the effects of the other motors and the external force on the cargo, the forward stepping rate (indicated by “+”) for a motor within the cluster can be written as

$$r_i^+ = r_0^+ e^{-\frac{\Delta V_0 + \Delta V_{\text{ext}} + \Delta V_{\text{int},i}}{k_B T}} = r_0^+ e^{-\frac{\Delta V_0}{k_B T}} \underbrace{e^{\frac{F_{\text{ext}} d}{N \kappa_m k_B T}}}_{\delta_{\text{ext}}^+} \underbrace{e^{\frac{-\kappa d^2}{2 k_B T}}}_{\delta_{\kappa}^+} \underbrace{e^{\frac{-\kappa y_{\text{int},i} d}{k_B T}}}_{\delta_{y,i}^+}. \quad (1)$$

This rate is the product of the zero-load stepping rate of an individual motor r_m^+ and factors which reflect the effect of the external forces δ_{ext}^+ , the interaction of the i th motor with the other motors $\delta_{y,i}^+$, and the spatial variation of the intermotor forces δ_{κ}^+ . In the presence of highly counteracting forces, molecular motors also perform backward steps [37], which can be treated equivalently to the forward steps using the substitutions $\Delta V_0 \rightarrow \Delta V_0 + \Delta V_{\text{ATP}}$, $d \rightarrow s_m - d$, and $F_{\text{ext}} \rightarrow -F_{\text{ext}}$. When we employ the individual motor rate $r_m^+ = \frac{v_m}{s_m}$, neither the diffusivity of the motor nor the barrier height ΔV_0 nor the exact shape of the potential need to be known explicitly. Assuming the same shape factor and diffusivity for the backward steps as for the forward steps, the backward stepping rate without load yields $r_m^- = r_m^+ e^{-\frac{\Delta V_{\text{ATP}}}{k_B T}}$, where the free energy difference between two minima of the motor potential $\Delta V_{\text{ATP}} = s_m F_{\text{stall}}$ is chosen to fit the maximal work an individual motor can perform per step.

C. Markov chain description

Assuming a continuous track for the motors, the system of coupled motors is invariant under translations of integer multiples of the step size s_m . Since the fluctuations of a motor in

one potential well are small in comparison to a motor step and on time scales, which are short in comparison to the dwell time of a motor, we assume that the effect of the other motors is well described by their temporal average. This mean-field approach leads to a discrete set of states of the motor cluster which are characterized by the number N of motors involved and the internal deflections $y_{\text{int},i}$ $i = 1, \dots, N$ [Fig. 1(c)] [17,19]. The ground state of a group of N motors is defined as the state with the narrowest distribution of deflections $\sigma = \frac{1}{N} \sqrt{\sum_{i=1}^N y_{\text{int},i}^2}$. In this context, we can define the individual motor phase $\varphi_i = y_{\text{int},i}/s_m$ by the motors' deflection $y_{\text{int},i}$ in the ground state relative to the step size. If one motor of the cluster performs a step, the system switches into another state. Equation (1) allows to calculate the stepping rate for each motor of the cluster and therefore the transition probabilities

$$p(k|\ell) = p^+(k|\ell) + p^-(k|\ell) \\ = r_m^+ \delta_{\text{ext}}^+ \delta_{\kappa}^+ \delta_{y,\mu(k,\ell)}^+ + r_m^- \delta_{\text{ext}}^- \delta_{\kappa}^- \delta_{y,\nu(k,\ell)}^- \quad (2)$$

from one state to another. Here, $\mu(k,\ell)$ and $\nu(k,\ell)$ refer to the motors performing a forward or backward step, which leads to a transition from state k to state ℓ . The time evolution of a system of a countable number of statistically switching states $P_k(t)$ can be described by the master equation

$$\frac{dP_k(t)}{dt} = \sum_{\ell} [p(\ell|k)P_{\ell}(t) - p(k|\ell)P_k(t)]. \quad (3)$$

The internal strain between the motors leads to a vanishing probability for states where the motors are distributed over a larger region, which corresponds to states with higher internal energy. Which of the states have a nonvanishing probability depends on molecular parameters such as the interaction stiffness κ . The states that need to be considered can be determined by iteratively taking states with higher internal strains into account until the probability to reach the states with the highest internal strains tends to zero. The time averaged probability distribution P_k is given by the stationary solution of the master equations $\sum_{\ell} [p(\ell|k)P_{\ell} - p(k|\ell)P_k] = 0 \forall k, \ell$. An exemplary calculation for a two-motor system is given in SM2 [36].

III. NUMERICAL SIMULATIONS

Alternatively to the description based on Kramers rates and Markov chains, the system of coupled molecular motors can also be treated by simulating the diffusive behavior of the motors and the cargo by means of a Brownian dynamics simulation. As introduced before, we described a step of a molecular motor by a diffusion over a potential barrier. Such a diffusion of the motor coordinate x in the motor's potential landscape can be described by the Langevin equation

$$F_{\text{th},m}(t) = -\gamma_m \dot{x}(t) - \nabla V_0(x) + F_c(x, x_c), \quad (4)$$

which takes the form of a Newtonian equation of motion for an overdamped particle that is subject to a fluctuating force. Here, γ_m is the viscous drag of the motor, $F_c = \kappa_m[x(t) - x_c(t)]$ is the force of the cargo at position x_c on the motor at position x , and F_{th} is the thermal force. The amplitude of this rapidly fluctuating random force is described by the fluctuation-dissipation theorem $\langle F_{\text{th},m}(t) F_{\text{th},m}(t + \tau) \rangle =$

$2\gamma_m k_B T \delta(\tau)$, where k_B is the Boltzmann constant, $T = 310$ K is the temperature, and $\delta(\tau)$ is the Dirac delta function [38]. Here, the delta function $\delta(\tau)$ is an approximation for the actual random force which is assumed to have an infinitely short correlation time corresponding to the collision time between the molecules. The relative coordinate used in the Kramers description above can be derived by $y_i = x_i - x_c$, where $x_i = x_c$ indicates that there is no strain between the motor and the cargo. Thus, $x_i = x_j$ does not imply that the motors share a binding site, but that these motors have the same relative position and thus experience the same force from the cargo. The cargo position x_c projected onto the direction of the filament the molecular motors are connected to can be described by the Langevin equation

$$F_{\text{th},c}(t) = -\gamma_c \dot{x}_c(t) + F_{\text{ext}} - \sum_{i=1}^N \kappa_m [x_c(t) - x_i(t)], \quad (5)$$

which includes the cargo's friction force $\gamma_c \dot{x}_c(t)$, additional external forces F_{ext} acting on the cargo, and the sum of all motor forces $\sum_{i=1}^N \kappa_m [x_c(t) - x_i(t)]$. Here, N denotes the number of motors involved. The thermal force on the cargo $F_{\text{th},c}$ is assumed to be uncorrelated, i.e., $\langle F_{\text{th},c}(t) F_{\text{th},c}(t + \tau) \rangle = 2\gamma_c k_B T \delta(\tau)$. Equations (4) and (5) form a system of coupled Langevin equations, which are treated numerically using a Brownian dynamics simulation.

A. Forces appearing in the simulation

In order to perform the numerical simulation, all forces occurring in Eqs. (4) and (5) have to be calculated explicitly for every time step. Therefore, the different terms of these equations are analyzed in the following. Since the actual shape of the motor potential is unknown and differs for the various types of motor proteins, the simulation is based on the simplest possible potential complying with the premise given by the mentioned motor parameters (s_m , ΔV_0 , ΔV_{ATP} , and d), which is a sawtooth potential as illustrated in Fig. 1(b). This leads to piecewise constant forces

$$-\nabla V = \begin{cases} -\frac{\Delta V_0}{d} & \text{for } (x_i - s_m \varphi_i \bmod s_m) \in [0, d] \\ \frac{\Delta V_0 + \Delta V_{\text{ATP}}}{s_m - d} & \text{for } (x_i - s_m \varphi_i \bmod s_m) \in]d, s_m[\end{cases} \quad (6)$$

where φ_i is the phase of the i th motor. The height of the potential barrier ΔV_0 was adapted to fit the motor's rate $r_m^+ = \frac{v}{s_m}$ to perform a forward step. It should be noted that the potential shape affects both the velocity of a single motor as well as the coupling between the motors to a minor degree. The thermal force is derived from the fluctuation-dissipation theorem. The common way to approximate the delta distribution $\delta(\tau)$ in such kinds of equations numerically is to set it to $1/\Delta t$, if $\tau < \Delta t$ and otherwise to 0. This yields the stochastic thermal forces [39]

$$F_{\text{th},m} = r_n \sqrt{\frac{2\gamma_m k_B T}{\Delta t \langle r_n^2 \rangle}} \quad (7)$$

for the motors and

$$F_{\text{th},c} = r_n \sqrt{\frac{2\gamma_c k_B T}{\Delta t \langle r_n^2 \rangle}} \quad (8)$$

for the cargo, where $\langle r_n^2 \rangle$ is the variance of the distribution of the random variable r_n , which is produced by a random number generator. In this context, the external force F_{ext} describes the additional forces on the cargo. The interaction between a motor and the cargo is modeled by a Hookean spring with stiffness κ_m . The force a motor applies on the cargo and vice versa is therefore given by $\kappa_m(x_{c,n} - x_{i,n})$. The absolute values of the friction coefficients γ_m and γ_c scale the time step [see Eq. (9)]. In this context, the coupled motor system is described by a system of coupled Brownian particles. Since only the general behavior of such a system is of interest, the system can be scaled without influencing the resulting behavior. Thus, the friction parameters γ_m and γ_c can be scaled without affecting the simulation results, as long as the autocorrelation time τ_{AC} of the fluctuation of the motor's position in its potential well is short in comparison to the rest time τ_R of a motor.

B. Simulation iteration procedure

The Brownian dynamics simulation iteration procedure can be derived from Eqs. (4) and (5) by approximation of the temporal derivative of the position coordinates x and x_c by their difference quotients with a nonvanishing time step Δt . This yields the iteration step

$$x_{i,n+1} = x_{i,n} + [-\nabla V(x_{i,n}) - \kappa_m(x_{i,n} - x_{c,n}) - F_{\text{th},i}] \frac{\Delta t}{\gamma_m} \quad (9)$$

for the motor positions and

$$x_{c,n+1} = x_{c,n} + \left[F_{\text{ext}} - \sum_{i=1}^N \kappa_m(x_{c,n} - x_{i,n}) - F_{\text{th},c} \right] \frac{\Delta t}{\gamma_c} \quad (10)$$

for the cargo position. Here, the index n indicates the iteration and the index i indicates the motor number. The iteration steps for the motor positions (9) and for the cargo position (10) are calculated successively.

IV. RESULTS

A. Cargo velocity

Since the velocity of a cargo can be measured easily, it is the most obvious observable of a motor cluster. The velocity as a function of the counteracting force is often experimentally accessible both for individual and coupled motors [32,40–42]. From the presented model, the cargo velocity and thus the mean motor velocity

$$v = \frac{s_m}{N} \sum_{k,\ell} [p^+(k|\ell) - p^-(k|\ell)] P_k \quad (11)$$

can be derived from the transition probabilities $p^{+/-}(k|\ell)$ between the states weighted by the probability P_k to find the system in the corresponding state k . $\frac{s_m}{N}$ is the substep size, i.e., the displacement of the cargo when one motor out of N

performs a step. The Brownian dynamics simulations provide directly the velocity of the cargo. The resulting velocities shown in Figs. 3 and 4 are extracted from the analysis of traces of 10 s length. The error bars correspond to the statistical errors of the simulated motor steps.

B. Synchronization

The linear processive motors considered in this work move in a stepwise behavior along their filaments. Apart from the motors' velocity and the load they can pull, the stepwise behavior revealed from high-precision measurements provides a detailed insight into the structure and function of these motor proteins. If all motors involved in the transport of a cargo perform their steps almost at the same points in time, these motors synchronize their steps.

The better the step synchronization, the longer the time τ_R the motor system rests in a preferred state (i.e., the ground state) relative to the time τ_D the system needs to perform an entire step of step size s_m (see Fig. 2). Thus, the synchronization

$$q = \left\langle \frac{\tau_R}{\tau_D} \right\rangle = \frac{\langle \tau_R v \rangle}{s_m} \quad (12)$$

can be defined as the expectation value of the ratio of τ_R to $\tau_D = s_m/v$. After an entire step has been performed the system has usually returned to the ground state. Therefore, the synchronization can be identified as the probability P_0 to find the system in the ground state. q is a dimensionless parameter smaller than 1, where a perfect synchronization results in $q = 1$. The synchronizations resulting from the Brownian dynamics simulations can be obtained directly from the fraction of time the system spent in the ground state.

C. Selected molecular parameters

The presented Kramers rate approach as well as the numerical simulations provide observables that can be compared to results from modern molecular motor experiments [35]. The velocity, the force dependency, and the synchronization of coupled molecular motors are analyzed exemplarily for

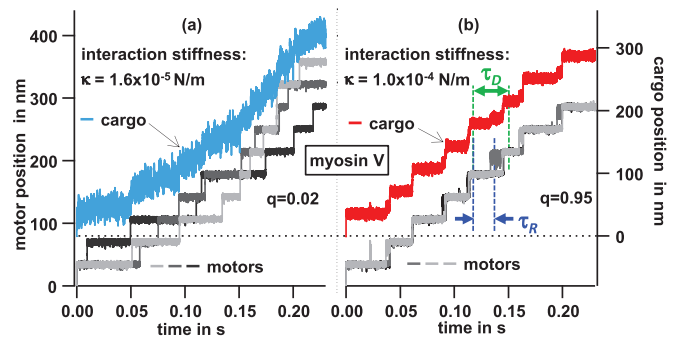


FIG. 2. (Color online) Traces of cargo and motors as a function of time. Traces resulting from Brownian dynamics simulations of three myosin V motors with step size $s_m = 36$ nm (lower lines in gray, left axes) that pull on a cargo (upper lines in blue and red, right axes) in the absence of an external force on the cargo for low (a) and high (b) coupling stiffness.

TABLE I. Literature values of parameters characterizing the motor proteins myosin V and kinesin I.

Observable measure	Myosin V	Kinesin I	References
Step size s_m	36 nm	8 nm	[26,43–45]
Stall force F_{stall}	2.3 pN	6.2 pN	[32,44–47]
Distance parameter d	4.3 nm	1.3 nm ^a	[45,47,48]
Single mol. velocity v_m	350 nm/s	800 nm/s	[32,44,49]
Vesicle velocity v	450 – 1800 nm/s	3500 – 4000 nm/s	[50–52]

^aThe value for the distance parameter d of kinesin I is selected to fit the measurements of Ref. [45].

the processive motors myosin V and kinesin I. The specific literature parameters of these proteins as listed in Table I are applied for both the Kramers description and the numerical simulation.

D. Change in transport efficiency due to coupling

In general, the effect of the load on several motors cannot be described by scaling the effects of a single motor since the ratio between the different stepping probabilities changes. For low coupling stiffnesses κ , the velocity-force relation is similar to the case of an individual motor (SM3 in Ref. [36]) scaled by the number N of motors involved (in accordance to [53]). Thus, calculating Eq. (11) reveals that a weakly coupled two-motor system decreases in cargo velocity v until a counteracting force F_{ext} of approximately twice the stall force F_{stall} of an individual motor is reached (see Table I and Fig. 3). This additive behavior of F_{stall} agrees well with experimental studies [54–57]. However, for stronger motor couplings, the mean step rate of the motors and thus the velocity decays stronger with F_{ext} . This effect becomes more obvious when considering the

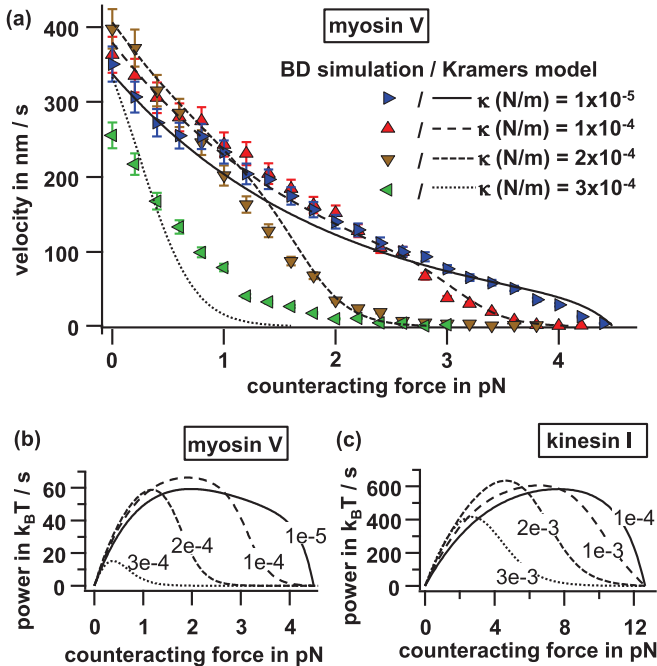


FIG. 3. (Color online) (a) Mean velocity of a system of two myosin V motors in phase as a function of the load F_{ext} for different coupling stiffnesses κ . (b) Power expended by two coupled myosin V motors as a function of F_{ext} for different κ (in N/m). (c) Same as (b) for two coupled kinesin I motors.

power $\Omega = F v$ expended by the motors, which is maximal at a certain load. The maxima in Ω are shifted for different κ as shown in Figs. 3(b) and 3(c). Thus, an intermediate coupling strength is favorable to carry low loads. However, the intermotor coupling must be reduced in order to carry higher loads efficiently. Hence, a variation of κ might regulate intracellular cargo transport in terms of maximum loading, velocity, and efficiency.

E. Increased transport velocity

As shown in Fig. 4, the velocity v of a motor cluster depends on the coupling stiffness κ in a complex manner. In the case of motors in phase, v increases with increasing κ until a maximum is reached (see SM4 in Ref. [36] for off-phase motors). With an increasing number N of motors involved, the maximum of

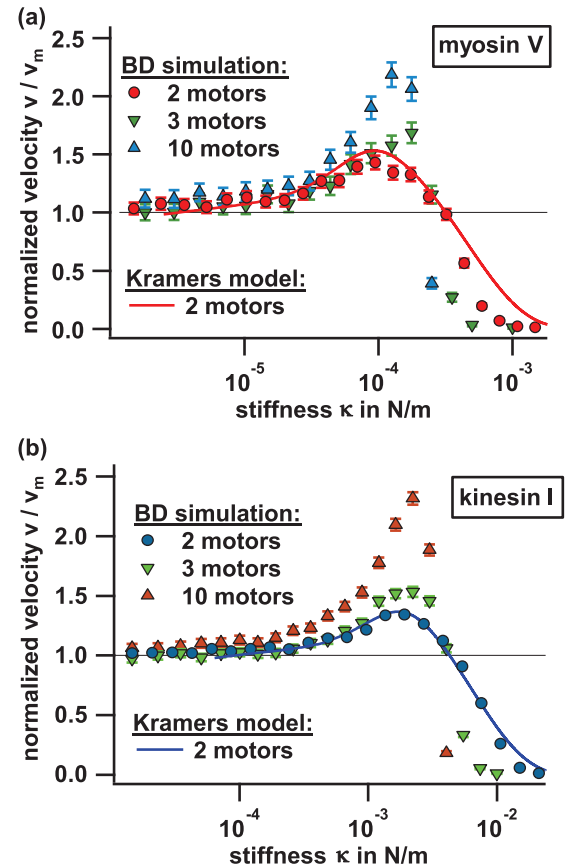


FIG. 4. (Color online) Normalized mean cargo velocities v/v_m of coupled myosin V motors (a) and coupled kinesin I (b) motors in phase in dependence of the coupling stiffness κ .

$v(\kappa)$ becomes more pronounced. This positive interference of the motors can be explained by the fact that a leading motor pulls on the other motor(s) and increases the probability for the trailing motor(s) to perform a step [20,21]. However, very high coupling stiffnesses impede the initial step of a motor [term δ_κ^+ in Eq. (1)] thus reducing the step rate and $v(\kappa)$. In the case of motors out of phase, the drop in velocity for high coupling stiffnesses is attenuated or disappears (see SM4 in Ref. [36]). However, interaction stiffnesses that are too high might increase the unbinding probability of the motors, a case that is not considered in our model. It seems reasonable that the induced unbinding of motors also leads to a reduction of the velocity for high coupling stiffnesses—an effect which should be addressed in future studies.

The dependency of the velocity on the motor coupling might help to explain the paradox situation that vesicles inside cells maneuver with velocities that exceed those of the respective single motors (see Table I). *In vitro* motility assays of coupled molecular motors reveal both an increase [12] as well as a decrease [13] in transport velocity in comparison to measured individual motor velocities. Interestingly, the measured stiffness of 0.34 ± 0.08 pN/nm of the linkage of kinesin I to a bead [58] corresponds approximately to the peak of the group velocity of kinesins shown in Fig. 4. Hence, depending on the predominant demands inside the cell, different coupling strengths seem to be favorable for an efficient cargo transport.

F. Motor synchronization

In recent experiments, it has been shown that the step size of organelles pulled by several kinesin or dynein motors corresponds to the step size of the individual motor proteins (8 nm) [59]. These findings indicate a strong coupling and a synchronization of the motor proteins, since otherwise substeps of fractional step sizes as reported in Refs. [8,60,61] should dominate. As illustrated in Fig. 2, the trace of a cargo pulled by a motor cluster is influenced significantly by the degree of motor synchronization q . The stepping of synchronized motors leads to clear steps in the trace of the cargo, where the step size corresponds to the one of the individual motors. For a low q , substeps, i.e., steps of one or a few motors involved, gain in relevance, although it can be difficult to determine the individual substeps. For $q > 0.5$, where the time τ_R in the ground state can be determined and where states with the same emission parameter of the hidden Markov model as the ground state, i.e., the cargo position, are negligible, the synchronization is observable by analysis of the cargo trace. However, the synchronization can be analyzed in a wider range by means of methods where individual motor proteins are labeled [9,42].

Depending on the specific molecular motor parameters, the synchronization increases nonlinearly with the coupling strength κ [Fig. 5(a)]. The calculated synchronization corresponds well to the simulation results, which are extracted from the analysis of traces of 10 s length. With increasing κ , the higher-energy states depopulate and $q = 1 - \sum_{i=1}^4 P_i$ quickly approaches 1.

More interestingly, the velocity at zero load reveals a maximum at a certain synchronization, which depends on the

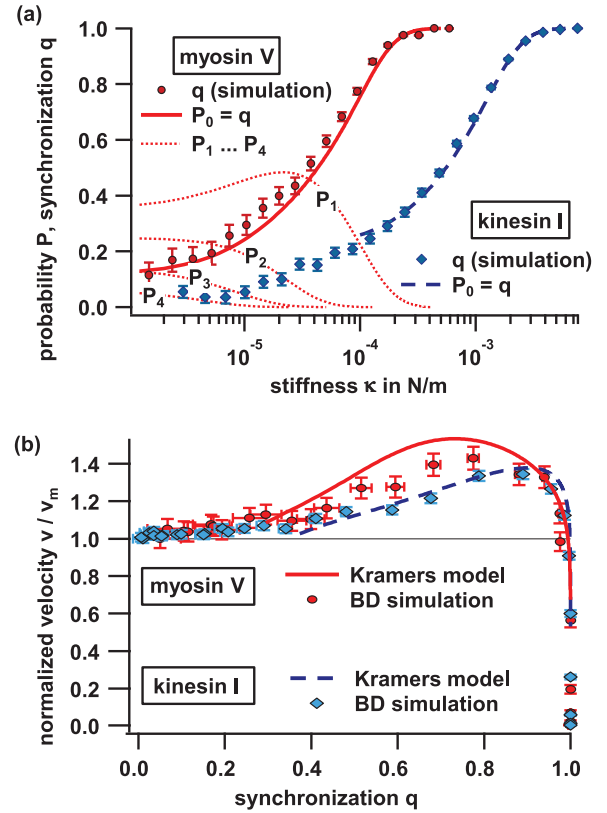


FIG. 5. (Color online) (a) Synchronization $q = P_0$ of two coupled myosin V (kinesin I) motors in phase as function of the coupling stiffness κ . For the case of myosin V, the probabilities $P - P_4$ to find the system in the states 1–4 (see SM2 [36]) are shown in addition. (b) Normalized velocity as a function of the synchronization.

type of motor [$q = 0.75$ for myosin V, $q = 0.9$ for kinesin I; see Fig. 5(b)]. The increased cargo velocity results from an enhanced stepping rate of the trailing motors for large enough κ or q , respectively. This seems to be more effective than the reduction of the stepping rate of the leading motors. However, for a coupling of the motors that is too strong ($q \rightarrow 1$), the massive interaction prevents an initial step of a motor according to $\delta_\kappa^+ = e^{-\frac{\kappa d^2}{2k_B T}}$ in Eq. (1), which reduces the velocity. Once the number of motors is determined by the ratio of the step size to the substep size, the results described can be used to determine molecular parameters, such as the interaction stiffness. The alternative measure “synchronization” encodes motor cooperativity and coupling based on molecular motor properties. In this way, it serves as a measure for molecular self-organization, which has been difficult to quantify so far.

V. CONCLUSION

We have described the coordinated transport of a cargo by several elastically coupled motors using a Markov chain model and rate transitions in a multiwell energy landscape, which is specific for different motors such as myosin V or kinesin I. We have introduced the synchronization parameter q as an observable, which identifies the coupling between the motors involved. This intermotor synchronization is defined as the probability to find the motor system in its ground

state and, in principle, can be extracted directly from cargo trajectories. Our description allows to estimate nonlinear relationships between loading force and velocity or power for different coupling strengths. We have shown that the cargo velocity increases to a maximum with increasing motor synchronization until the cargo stops for full synchronization. The synchronization described here results from the mutual influences of repetitive stochastic molecular processes, which play a significant role for self-organization in many biological systems. Our work enables a comparison between theories and measurements of intermotor coupling. Thereby it helps

to identify motor coupling during cargo transport in fluctuation trajectories measured in both *in vivo* and *in vitro* systems.

ACKNOWLEDGMENTS

We thank Professor Gerhard Stock and Felix Jünger for proofreading the manuscript. This study was supported by the Excellence Initiative of the German Federal and State Governments (EXC 294) and by the Deutsche Forschungsgemeinschaft (DFG), Grant No. RO 3615/3.

-
- [1] J. Howard, *Mechanics of Motor Proteins and the Cytoskeleton* (Sinauer Associates, Sunderland, MA, 2001).
- [2] D. Keller and C. Bustamante, *Biophys. J.* **78**, 541 (2000).
- [3] F. Jülicher and J. Prost, *Phys. Rev. Lett.* **75**, 2618 (1995).
- [4] S. P. Gross, M. Vershinin, and G. T. Shubeita, *Curr. Biol.* **17**, R478 (2007).
- [5] C. M. Brawley and R. S. Rock, *Proc. Natl. Acad. Sci. USA* **106**, 9685 (2009).
- [6] M. Y. Ali, E. B. Kremenstova, G. G. Kennedy, R. Mahaffy, T. D. Pollard, K. M. Trybus, and D. M. Warshaw, *Proc. Natl. Acad. Sci. USA* **104**, 4332 (2007).
- [7] T. Guérin, J. Prost, P. Martin, and J.-F. Joanny, *Curr. Opin. Cell Biol.* **22**, 14 (2010).
- [8] C. Leduc, F. Ruhnow, J. Howard, and S. Diez, *Proc. Natl. Acad. Sci. USA* **104**, 10847 (2007).
- [9] M. Y. Ali, G. G. Kennedy, D. Safer, K. M. Trybus, H. L. Sweeney, and D. M. Warshaw, *Proc. Natl. Acad. Sci. USA* **108**, E535 (2011).
- [10] X. Nan, P. A. Sims, P. Chen, and X. S. Xie, *J. Phys. Chem. B* **109**, 24220 (2005).
- [11] H. Kress, E. H. K. Stelzer, D. Holzer, F. Buss, G. Griffiths, and A. Rohrbach, *Proc. Natl. Acad. Sci. USA* **104**, 11633 (2007).
- [12] P. Bieling, I. A. Telley, J. Piehler, and T. Surrey, *EMBO Rep.* **9**, 1121 (2008).
- [13] J. Gagliano, M. Walb, B. Blaker, J. C. Macosko, and G. Holzwarth, *Eur. Biophys. J.* **39**, 801 (2010).
- [14] S. Klumpp and R. Lipowsky, *Proc. Natl. Acad. Sci. USA* **102**, 17284 (2005).
- [15] C. B. Korn, S. Klumpp, R. Lipowsky, and U. S. Schwarz, *J. Chem. Phys.* **131**, 245107 (2009).
- [16] F. Berger, C. Keller, M. J. I. Müller, S. Klumpp, and R. Lipowsky, *Biochem. Soc. Trans.* **39**, 1211 (2011).
- [17] F. Berger, C. Keller, S. Klumpp, and R. Lipowsky, *Phys. Rev. Lett.* **108**, 208101 (2012).
- [18] F. Berger, M. J. I. Müller, and R. Lipowsky, *EPL (Europhysics Lett.)* **87**, 28002 (2009).
- [19] Z. Wang and M. Li, *Phys. Rev. E* **80**, 041923 (2009).
- [20] Y. Zhang, *Phys. Rev. E* **83**, 011909 (2011).
- [21] M. Evstigneev, S. von Gehlen, and P. Reimann, *Phys. Rev. E* **79**, 011116 (2009).
- [22] J. G. Orlandi, C. Blanch-Mercader, J. Brugués, and J. Casademunt, *Phys. Rev. E* **82**, 061903 (2010).
- [23] J. Brugués and J. Casademunt, *Phys. Rev. Lett.* **102**, 118104 (2009).
- [24] P. Margaretti, I. Pagonabarraga, and D. Frenkel, *Phys. Rev. Lett.* **109**, 168101 (2012).
- [25] J. W. Driver, D. K. Jamison, K. Uppulury, A. R. Rogers, A. B. Kolomeisky, and M. R. Diehl, *Biophys. J.* **101**, 386 (2011).
- [26] A. Yildiz, M. Tomishige, R. D. Vale, and P. R. Selvin, *Science* **303**, 676 (2004).
- [27] E. Toprak, A. Yildiz, M. T. Hoffman, S. S. Rosenfeld, and P. R. Selvin, *Proc. Natl. Acad. Sci. USA* **106**, 12717 (2009).
- [28] C. Veigel, F. Wang, M. L. Bartoo, J. R. Sellers, and J. E. Molloy, *Nat. Cell Biol.* **4**, 59 (2002).
- [29] J. M. Berg, J. L. Tymoczko, and L. Stryer, *Biochemistry*, 5th ed. (W.H. Freeman and Company, New York, 2002).
- [30] H. Kramers, *Physica* **7**, 284 (1940).
- [31] H. C. Brinkman, *Physica* **22**, 149 (1956).
- [32] K. Visscher, M. J. Schnitzer, and S. M. Block, *Nature* **400**, 184 (1999).
- [33] A. Kunwar, M. Vershinin, J. Xu, and S. P. Gross, *Curr. Biol.* **18**, 1173 (2008).
- [34] M. R. Diehl, K. Zhang, H. J. Lee, and D. A. Tirrell, *Science* **311**, 1468 (2006).
- [35] E. L. F. Holzbaur and Y. E. Goldman, *Curr. Opin. Cell Biol.* **22**, 4 (2010).
- [36] See Supplemental Material at <http://link.aps.org/supplemental/10.1103/PhysRevE.91.012701> for effective interaction stiffness, Markov chain description for two motors in phase, single motor behavior, and description of motors out of phase.
- [37] N. J. Carter and R. A. Cross, *Nature* **435**, 308 (2005).
- [38] R. Kubo, M. Toda, and N. Hasitsume, *Statistical Physics II: Nonequilibrium Statistical Mechanics* (Springer, Heidelberg, 1985).
- [39] P. S. Grassia, E. J. Hinch, and L. C. Nitsche, *J. Fluid* **282**, 373 (1995).
- [40] S. Block and L. Goldstein, *Nature* **348**, 348 (1990).
- [41] K. Furuta, A. Furuta, Y. Y. Toyoshima, M. Amino, K. Oiwa, and H. Kojima, *Proc. Natl. Acad. Sci. USA* **110**, 501 (2012).
- [42] H. Lu, A. K. Efremov, C. S. Bookwalter, E. B. Kremenstova, J. W. Driver, K. M. Trybus, and M. R. Diehl, *J. Biol. Chem.* **287**, 27753 (2012).
- [43] K. Svoboda, C. F. Schmidt, B. J. Schnapp, and S. M. Block, *Nature* **365**, 721 (1993).

- [44] A. D. Mehta, R. S. Rock, M. Rief, J. A. Spudich, M. S. Mooseker, and R. E. Cheney, *Nature* **400**, 590 (1999).
- [45] K. Svoboda and S. M. Block, *Cell* **77**, 773 (1994).
- [46] G. Cappello, P. Pierobon, C. Symonds, L. Busoni, J. C. M. Gebhardt, M. Rief, and J. Prost, *Proc. Natl. Acad. Sci. USA* **104**, 15328 (2007).
- [47] A. E.-M. Clemen, M. Vilfan, J. Jaud, J. Zhang, M. Bärmann, and M. Rief, *Biophys. J.* **88**, 4402 (2005).
- [48] C. Veigel, S. Schmitz, F. Wang, and J. R. Sellers, *Nat. Cell Biol.* **7**, 861 (2005).
- [49] M. Rief, R. S. Rock, A. D. Mehta, M. S. Mooseker, R. E. Cheney, and J. A. Spudich, *Proc. Natl. Acad. Sci. USA* **97**, 9482 (2000).
- [50] V. Levi, V. I. Gelfand, A. S. Serpinskaya, and E. Gratton, *Biophys. J.* **90**, L07 (2006).
- [51] R. D. Allen, J. Metzels, I. Tasaki, S. T. Brady, and S. P. Gilbert, *Science* **218**, 1127 (1982).
- [52] H. M. Zhou, I. Brust-Mascher, and J. M. Scholey, *J. Neurosci.* **21**, 3749 (2001).
- [53] T. L. Fallesen, J. C. Macosko, and G. Holzwarth, *Eur. Biophys. J.* **40**, 1071 (2011).
- [54] M. Vershinin, B. C. Carter, D. S. Razafsky, S. J. King, and S. P. Gross, *Proc. Natl. Acad. Sci. USA* **104**, 87 (2007).
- [55] R. Mallik, D. Petrov, S. A. Lex, S. J. King, and S. P. Gross, *Curr. Biol.* **15**, 2075 (2005).
- [56] T. Fallesen, J. Macosko, and G. Holzwarth, *Phys. Rev. E* **83**, 011918 (2011).
- [57] C. Leidel, R. A. Longoria, F. M. Gutierrez, and G. T. Shubeita, *Biophys. J.* **103**, 492 (2012).
- [58] H. Kojima, E. Muto, H. Higuchi, and T. Yanagida, *Biophys. J.* **73**, 2012 (1997).
- [59] C. Kural, H. Kim, S. Syed, G. Goshima, V. I. Gelfand, and P. R. Selvin, *Science* **308**, 1469 (2005).
- [60] A. R. Rogers, J. W. Driver, P. E. Constantinou, D. K. Jamison, and M. R. Diehl, *Phys. Chem. Chem. Phys.* **11**, 4882 (2009).
- [61] D. K. Jamison, J. W. Driver, A. R. Rogers, P. E. Constantinou, and M. R. Diehl, *Biophys. J.* **99**, 2967 (2010).